Journal of Sound and Vibration 527 (2022) 116849

Contents lists available at ScienceDirect

Journal of Sound and Vibration

journal homepage: www.elsevier.com/locate/jsvi

In-process impulse response of milling to identify stability properties by signal processing

Adam K. Kiss [a,*], David Hajdu [a], Daniel Bachrathy [a], Gabor Stepan [b], Zoltan Dombovari [a]

[a] MTA-BME Lendület Machine Tool Vibration Research Group, Department of Applied Mechanics, Faculty of Mechanical Engineering, Budapest University of Technology and Economics, Budapest, Hungary

[b] Department of Applied Mechanics, Faculty of Mechanical Engineering, Budapest University of Technology and Economics, Hungary

ARTICLE INFO

Keywords:
Stability
Signal processing
In-process impulse response
Floquet multiplier
Milling
Chatter detection

ABSTRACT

In this work we present a quantitative measurement-based method to describe the stability behaviour of a periodic dynamical system. In-process response for impulse during milling is analysed to provide operational stability prediction. The proposed method combines chatter detection techniques with the theory of time-periodic delay differential equations applied for general milling operations. Signal processing based on dynamic modal decomposition approach not only presents qualitative properties (like stability/instability) but also quantifies a measure of stability through the determination of the Floquet multipliers. The corresponding monodromy operator of the milling process is approximated from the measured system's response during machining operation. By changing the technological parameters, the variation of the modulus of the Floquet multipliers can be monitored. The stability limit can precisely be interpolated with the unitary multiplier; furthermore, the stability limit can be extrapolated while the manufacturing parameters remain in the chatter-free region. The presented approach is validated by numerical results and laboratory tests.

1. Introduction

In the manufacturing industry, productivity is a crucial factor besides quality, efficiency and sustainability. However, productivity cannot be increased arbitrarily due to undesired vibrations that may arise during the cutting processes. The most critical form of vibrations is called chatter, which can lead to extensive tool wear, unacceptable surface quality or even possible damage in the components of the machine-tool [1]. Over the past six decades, a significant number of studies have dealt with the study of chatter and productivity, yet the prediction and avoidance of these vibrations are still an open area of research [2]. Therefore, it is an essential task for mechanical engineers to predict the dynamic behaviour of a machining process to achieve high material removal rates, thus increasing the production rate in manufacturing while also avoiding chatter [3].

One of the most common methods to avoid unwanted vibrations is to use the so-called stability charts that separate the chatter-free (stable) and chatter (which is said to be unstable) parameter domains. The calculation techniques of these charts are based on the mathematical modelling of the milling process. It is well-known that the regenerative effect [4] is responsible for the occurrence of chatter, namely, the past vibrations of the tool affects the instantaneous chip thickness, thus the cutting force [5]. It can be modelled by delay-differential equations (DDEs) [6] subjected to time-periodicity, and the Floquet theory describes their stability

* Corresponding author.
E-mail address: kiss_a@mm.bme.hu (A.K. Kiss).

https://doi.org/10.1016/j.jsv.2022.116849
Received 17 August 2021; Received in revised form 7 February 2022; Accepted 12 February 2022
Available online 24 February 2022

properties [7]. Although highly developed numerical techniques exist that can produce stability charts in seconds as collected in [8], uncertainties can occur both in the dynamic description of the system's behaviour and in the modelling of the cutting force [9–12]. These uncertainties affect model coefficients and may result in unreliable stability charts. Another limitation of the usage of stability lobe diagrams is that it is calculated prior to the beginning of the manufacturing process, thus it is not suitable for tracking changes during the cutting process (such as tool wear, change in material characteristics due to temperature variance and/or changing dynamical properties along complex tool paths) [13]. Consequently, it is considered as an out-of-process strategy of low reliability for chatter avoidance [14].

Meanwhile, according to [14], in-process strategies include chatter detection techniques and in case of unwanted vibrations, the technological parameters are tuned during the milling process to reach stable operation. Online chatter detection techniques are essential elements of active chatter suppression methods, which are based on real-time signal processing and distinguish between chatter-free and chatter machining processes. These techniques usually give qualitative conditions to the stability of milling processes, whether it is stable or not [15–17]. A novel detection technique is presented in [18], where a qualitative measure was introduced for chatter detection that is based on the deviation of periodic sampling of signals. In almost all chatter detection methods, the separation of stable and unstable operations is based on so-called chatter indicators [19–22]. These are usually measurement-based indicators that can be determined in different ways for each method. The signal processing of the measurement data for the different indicators can take place in both time and frequency domain. The chatter indicators can be categorized as classical statistical methods like standard deviation or peak-to-peak amplitude, and traditional methods as fast fourier transformation and power spectral density which try to capture the energy ratio of the chatter vibration components. Also, the critical levels of the indicators (thresholds) are usually defined empirically. Therefore, these thresholds are typically determined by human experts based on preliminarily measured datasets. Also, they do not use directly the stability theory behind the milling operation. A comprehensive literature review about chatter detection can be found in [14] and all the references therein.

Our idea is to propose a method that combines the chatter detection techniques with the theory of time-periodic delay differential equations, in other words, where the chatter detection method meets the Floquet theory. This technique is not based on an experimentally tuned threshold, but on a quantity associated with the theory of periodic delay differential equations. This quantity is the so-called Floquet multiplier, which characterizes the exponential growth of the solutions associated with the underlying delayed periodic systems. The system is stable if the magnitude of all the multipliers are smaller than one, otherwise it is unstable. Consequently, one can quantify from measurement data how stable or unstable the milling process is.

In other words, the main goal of this research is to characterize the dynamical behaviour of delayed periodic systems (e.g., a milling operation) without essential knowledge of the parameters of the underlying mechanical model. The main idea is to measure the so-called dominant spectral properties of the system which characterize the behaviour during milling operation. To obtain them from experiments, it requires additional excitation under stable machining condition, where the resultant transient vibration has to be captured. This measurable transient onset vibration 'connects' the stationary milling operation to the large amplitude chatter vibration.

According to the Floquet theory, the multipliers are the eigenvalues of the corresponding monodromy operator. Due to the nature of time-delay systems, this operator has infinite dimensions [6], but it can be approximated by the finite-dimensional monodromy matrix [23]. For this, we reduce the infinite-dimensional system to a finite-dimensional one in which the dominant behaviour is relevant. In the literature, it is usually referred to as reduced-order modelling (ROM) [24].

There are different methods for ROM and in what follows is a summary of those which are suitable to be applied for milling. In [25], the authors used spectral discretization and the Krylov subspace to approximate the infinite domain with finite one. Another technique, the so-called proper orthogonal decomposition (POD), is a powerful dimension reduction technique [26], which is also called in the literature as empirical orthogonal eigenfunction (EOF) analysis, principal component analysis (PCA) or Karhunen–Loeve decomposition (KLD). It is based on an energy ranking of orthogonal structures computed from a correlation (also called covariance) matrix by means of singular value decomposition, where the energy ranking is given by the singular values. Another suitable ROM technique is the so-called impulse dynamic subspace (IDS) method [27,28], which uses singular value decomposition in order to capture the dominant spectral properties and to provide a system matrix without modelling. Originally, this method was developed for linear time-invariant systems, and its slightly modified version in [29] is applicable also for periodic delayed systems.

Another technique is the dynamic mode decomposition (DMD), which can approximate the monodromy operator in least mean square sense. Initially, the DMD method was developed to decompose fluid flows and to find coherent structures in [30]. Then it became well-used in several fields like studying large-scale neural activity in [31], investigating cyclic behaviour in the stock market in [32], using for pattern recognition in infectious diseases in [33] or analysing systems with control input in [34], just to mention a few. Also, the DMD has been applied successfully for mechanical problems as a single-degree-of-freedom (SDoF) experiment in [35], and for a 2-DoF pendulum with no delay in [36]. In these mechanical examples, the dimension of the system is known in advance, however, the method can also be applied where the dimension of the system is unknown. These are typical for large-scale structures, flows that are modelled by partial differential equations (PDEs), and systems with time delay. The DMD method is applied for milling firstly in [37] and for periodic delayed systems with distributed delay in [38]. In [39] the POD and DMD methods are compared for delay systems, while recent improvement in the DMD method can be found in [40] where the influence of experimental noise is reduced significantly. A comprehensive literature review about the DMD method can be found in [41] and the references therein.

In this paper, we investigate the application of the DMD method for milling operations in a way that makes it capable to provide a quantitative measure of stability. Note that other ROM techniques may also be suitable for determining stability properties after being properly modified to handle periodic delay systems. Also note that in-process impulse excitation for inducing transient vibrations has already been used in [35,37,40,42], while operational modal analysis (OMA) was first applied and investigated to

estimate stability of turning processes in [43]. In case of OMA, the excitation relies on the cutting force mainly and also on random ambient noise.

The rest of the paper is organized as follows. The formalism of the DMD method is introduced in Section 2. Then, by using a case study, a demonstration of the proposed approach is presented in Section 3. Section 4 presents the major contribution of this work, which is the application of the method for milling processes. This section also describes the performance of the method and presents the possibilities of accurate stability limit prediction by means of interpolation and extrapolation. Finally, in Section 5, we conclude our results and discuss future research directions.

2. Dynamic modal decomposition

In this section, we recall the theory of linear time-periodic DDEs [23] and then we apply the DMD method in order to extract the Floquet multipliers. We provide the description for delayed systems, although in its original form, the method can be used directly for periodic non-delayed systems only.

2.1. Linear time-periodic DDEs

The general form of linear time-periodic differential equations with time delay τ reads

$$\dot{\mathbf{x}}(t) = \mathbf{L}(t, \mathbf{x}_t), \quad \mathbf{L}(t+T, .) = \mathbf{L}(t, .), \tag{1}$$

where $\mathbf{x} \in \mathbb{R}^n$ is the state variable and $\mathbf{x}_t$ represents all the possible delayed values. It is defined by the shift

$$\mathbf{x}_t(\theta) = \mathbf{x}(t+\theta), \quad \theta \in [-\tau, 0], \tag{2}$$

that is an element of the Banach space $\mathcal{B} = C([-\tau, 0], \mathbb{R}^n)$ representing the continuous functions in the interval $[-\tau, 0]$. $\mathbf{L} : \mathcal{B} \to \mathbb{R}^n$ is a continuous, T-periodic and linear functional; furthermore, T is the principal period. Here, the derivation will be presented for the case when the time delay is just equal to the principal period ($\tau = T$), which is typical for milling operations. Note that the derivation is valid for the case $\tau \leq T$ and it can also be extended for $\tau > T$. The solution of Eq. (1) with the initial function $\mathbf{x}_0$ is given by $\mathbf{x}_t = \mathcal{U}(t)\mathbf{x}_0$, where $\mathcal{U}(t)$ is the infinite-dimensional solution operator, which maps the solution t time later. According to periodic systems [7], the connection between the general state $\mathbf{x}_t$ and the state one principal period later $\mathbf{x}_{t+T}$ can be given by

$$\mathbf{x}_{t+T} = \mathcal{U}(T)\mathbf{x}_t, \tag{3}$$

where $\mathcal{U}(T) : \mathcal{B} \to \mathcal{B}$ is called the infinite-dimensional monodromy operator. Generally, the monodromy operator cannot be determined in closed form, but there exist several numerical and semi-analytical techniques to approximate it, such as in [23,44–46]. But one may want to approximate $\mathcal{U}(T)$ from measurement data where sampling is used. Thus, in the following, the DMD method is derived in details. The effect of the discretized state $\mathbf{x}_t(\theta)$ is presented through a test example.

2.2. Discretization in the DMD method

In this subsection, we present the mathematical background of the DMD method. Since our goal is to approximate the monodromy operator from sampled measurement data, here, we discretize time and approximate Eq. (3) with a discrete-time map. Let us define the time step $\Delta t = T/r$, $r \in \mathbb{N}$ yielding $\theta_l = -l\Delta t$, $l = 0, 1, \dots, r$. Thus, the equidistant discretization in period T of the state $\mathbf{x}_t(\theta)$ in Eq. (2) at the kth period can be defined as

$$\mathbf{z}_k := \mathrm{col}_l^r \, \mathbf{x}_{t+kT}(-l\Delta t) = \begin{bmatrix} \mathbf{x}(t+kT)^\top & \mathbf{x}(t+kT-\Delta t)^\top & \dots & \mathbf{x}(t+kT-(r-1)\Delta t)^\top \end{bmatrix}^\top, \ \mathbf{z}_k \in \mathbb{R}^{nr}, \ k \in \mathbb{N}. \tag{4}$$

In order to discretize Eq. (3), we use the Euler-type discretization scheme, but other choices of discretization can also be applied [23,47]. The monodromy operator $\mathcal{U}(T)$ is approximated by the finite-dimensional monodromy matrix $\mathbf{U} \in \mathbb{R}^{nr \times nr}$ (also called as principal matrix or transition matrix). Hence, for the finite-dimensional approximation of Eq. (3), the connection between the discretized state $\mathbf{z}_k$ and the discretized state $\mathbf{z}_{k+1}$ one period later can be given as

$$\mathbf{z}_{k+1} = \mathbf{U}\mathbf{z}_k. \tag{5}$$

The basic concept of the DMD method is to extend the monodromy mapping in Eq. (3) with K number of further elements [41]. Therefore let us introduce the following matrices composed from the discretized state $\mathbf{z}_k$ as

$$\mathbf{P} = \sum_{k=0}^{K} \mathbf{z}_k \mathbf{z}_k^\top, \quad \mathbf{Q} = \sum_{k=0}^{K} \mathbf{z}_{k+1} \mathbf{z}_k^\top, \quad \mathbf{P}, \mathbf{Q} \in \mathbb{R}^{nr \times nr}. \tag{6}$$

where $\mathbf{z}_{k+1}\mathbf{z}_k^\top$ denotes the dyadic product of two vectors. With these matrices, the mapping in Eq. (5) can be formed as

$$\mathbf{Q} = \mathbf{U}\mathbf{P}. \tag{7}$$

To extract the monodromy matrix $\mathbf{U}$, the inverse of $\mathbf{P}$ is needed, but due to the dyadic product in Eq. (6), $\mathbf{P}$ can have maximum $K+1$ nonsingular values. By choosing $K+1 \geq nr$, the monodromy matrix can be determined such as

$$\mathbf{U} = \mathbf{Q}\mathbf{P}^{-1}, \tag{8}$$

which provides the solution in linear least-square sense. Even with a proper selection of K, it is not guaranteed that $\mathbf{P}$ is invertible, however, these are special cases. In case of our measured data and simulations, only ill-conditioned matrices appear in some situations. Then the stability of the linear time-periodic DDEs in Eq. (1) can be approximated by the spectral radius of $\mathbf{U}$, which is computed based on the following eigenvalue problem

$$\det(\mu\mathbf{I} - \mathbf{U}) = 0, \tag{9}$$

where $\mathbf{I}$ is the identity matrix and μ_i, $(i = 1, 2, \dots, nr)$ are the characteristic multipliers (or Floquet multipliers) and they are ordered such that $i = 1$ corresponds to one with the largest modulus. Hence, Eq. (1) is exponentially stable if and only if all characteristic multipliers μ have modulus less than 1 ($|\mu_1| < 1$).

For the later validation of the DMD method, one needs to calculate the eigenvectors $\mathbf{s}_i$ of the matrix $\mathbf{U}$, which satisfy

$$\mathbf{U}\mathbf{s}_i = \mu_i \mathbf{s}_i. \tag{10}$$

Since $\mathbf{U}$ is the projection of the monodromy operator, eigenvectors $\mathbf{s}_i$ approximate the subspace of dominant modes, while eigenvalues μ_i estimate the dominant characteristic multipliers of the infinite dimensional monodromy operator $\mathcal{U}(T)$. Hence, with this discretization technique, one can obtain a finite-dimensional representation of the dynamics in Eq. (1).

It should be noted that using notation for the collected periods as $\mathbf{Z}_k = [\mathbf{z}_k\, \mathbf{z}_{k+1}\, \dots\, \mathbf{z}_{k+K}] \in \mathbb{R}^{nr\times K+1}$, the monodromy matrix can be given equivalently to Eq. (8) based on the pseudo inverse of $\mathbf{Z}_k$ as $\mathbf{U} = \mathbf{Z}_{k+1}\mathbf{Z}_k^\top(\mathbf{Z}_k\mathbf{Z}_k^\top)^{-1}$, which notation can be found in [30,36–40]. In this case, matrices $\mathbf{Z}_{k+1}\mathbf{Z}_k^\top$ and $\mathbf{Z}_k\mathbf{Z}_k^\top$ are equivalent to $\mathbf{Q}$ and $\mathbf{P}$, respectively.

2.3. Reconstruction of the dominant vibration signals

In this subsection we present the computation steps to reconstruct the signal belonging to the dominant multipliers and associated mode shapes. According to the eigenvalue problem presented in Eqs. (9) and Eq. (10), the monodromy matrix can be decomposed as

$$\mathbf{U} = \mathbf{S}\,\mathbf{M}\,\mathbf{S}^{-1}, \tag{11}$$

where matrix $\mathbf{M} = \mathrm{diag}_{j=1}^{nr}\mu_j$ contains the multipliers, matrix $\mathbf{S} = \mathrm{row}_{j=1}^{nr}\mathbf{s}_j$ collects the right eigenvectors $\mathbf{s}_j$ and matrix $\mathbf{S}^{-1} = \mathrm{col}_{j=1}^{nr}\mathbf{s}_{\mathrm{i},j}^\top$ organizes the left eigenvectors $\mathbf{s}_{\mathrm{i},j}^\top$. Then the corresponding monodromy matrix $\tilde{\mathbf{U}}$ mapping only the selected set of modes (j) can be reconstructed as

$$\tilde{\mathbf{U}} = \sum_j \mu_j \mathbf{s}_j \mathbf{s}_{\mathrm{i},j}^\top. \tag{12}$$

Note that in case of complex conjugate eigenvalue pairs e.g.: $\mu_{1,2}$, j must contain both components $j = \{1, 2\}$. Since this matrix contains information related to the considered modes only, the reconstructed vibration signals can be computed by

$$\tilde{\mathbf{Z}}_{k+1} = \tilde{\mathbf{U}}\mathbf{Z}_k, \tag{13}$$

where matrix $\tilde{\mathbf{Z}}_{k+1} = \mathrm{row}_{k=1}^{K}\tilde{\mathbf{z}}_{k+1}$ collects the reconstructed dominant vibration signals organized by T periods.

3. Validation by numerical simulation

In this section, convergence analysis of the discretization is presented based on a time-periodic delay-differential equation (DDE) which combines parametric forcing with time delay. In the DMD method, the discretization appears in two different ways: one is the number of the used discretized periods K in Eq. (6), second is the discretization of the state $\mathbf{x}_t$ along the period T in Eq. (4).

The method and its applicability is tested on the so-called delayed Mathieu equation (see [48,49]) by using time signal generated by numerical integration. The general form of the delayed Mathieu equation reads

$$\ddot{x}(t) + a_1\dot{x}(t) + (\delta + \varepsilon\cos t)\,x(t) = b_0 x(t-\tau), \tag{14}$$

where the time-period is $T = 2\pi$. Here, the special case is investigated, when the time delay is just equal to the principal period ($\tau = T$).

In order to validate the DMD method, the fitted dominant multipliers and the corresponding eigenvectors are compared directly to the theoretical ones ($\hat{\mu}_i$, $\hat{\mathbf{s}}_i$) calculated by the semi-discretization method (SDM) [23]. The DMD method is applied on numerically generated time signal shown in Fig. 1. The parameter set $\delta = 3.1605$, $\varepsilon = 1$, $a_1 = 0$, $b_0 = -0.6246$ are selected from the stability chart [23] close to the stability boundary. The applied initial conditions represent an impulse excitation of a stationary system, which reads as $[x_0(\theta)\ \dot{x}_0(\theta)]^\top = \mathbf{0}$ if $\theta \in [-\tau, 0)$ and $[x_0(0)\ \dot{x}_0(0)]^\top = [0\ \ 1]^\top$ if $\theta = 0$. The number of the simulated periods is 120 generated by absolute tolerance 10^{-16} and relative tolerance 10^{-5}. Then, the DMD method is applied based on the discretization steps described in Eqs. (4), (6) and (8).

First, the number of the considered periods in Eq. (6) is under investigation through the evolution of the fitted characteristic multipliers. Fig. 2a shows that the magnitudes of the fitted multipliers converge to constant values as the number of the considered

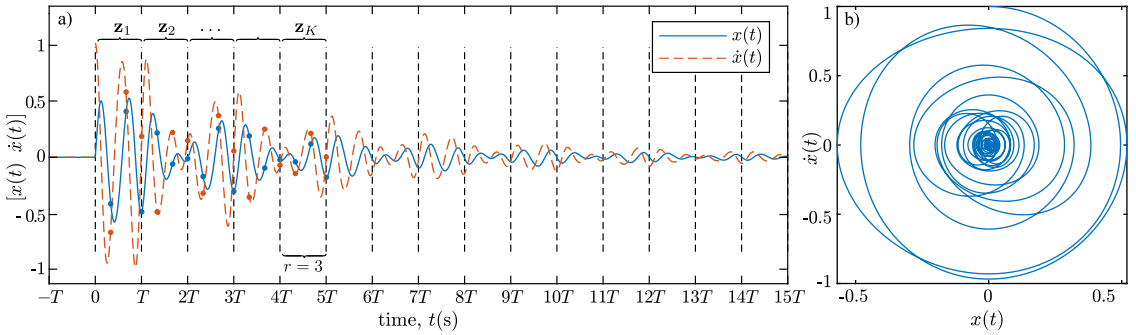

Fig. 1. Numerical simulation of the investigated delayed Mathieu equation. Panel (a) and (b) represent the time profile and phase portrait, respectively. Dots represent the discretization according to Eqs. (4) and (6). (For interpretation of the references to colour in this figure legend, the reader is referred to the web version of this article.)

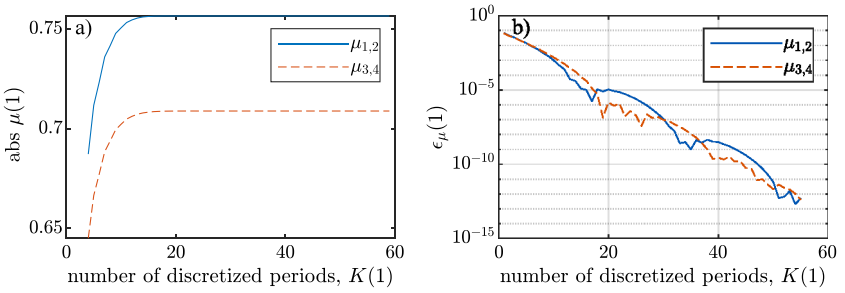

Fig. 2. Results of the fitted multiplier for the delayed Mathieu equation. Panel (a) represents the convergence of the fitted multiplier and panel (b) shows their relative errors defined in the function of considered periods for parameters $n = 2$ and $r = 2$. Note that there are complex conjugate eigenvalues ($\mu_1 = \overline{\mu}_2$). (For interpretation of the references to colour in this figure legend, the reader is referred to the web version of this article.)

periods is increased. Meanwhile Fig. 2b represents the relative errors in a logarithmic scale for the fitted multipliers. The relative error of the ith multiplier is defined by

$$\epsilon_{\mu,i}(K) = \frac{|\mu_{i,K} - \hat{\mu}_i|}{|\hat{\mu}_i|}, \tag{15}$$

where $\mu_{i,K}$ is the calculated multiplier with the DMD method considering K number of periods while $\hat{\mu}_i$ is considered as the exact multiplier calculated by the SDM method [23] with very high accuracy. It is easy to show that the relative error decreases by increasing the number of considered periods. From Fig. 2b, one can select an appropriate number of considered periods to keep the relative error within a desired range. For further investigation, we select 50 periods in this example.

As a next step, the effects of the discretization of the state $\mathbf{x}_t$ along the period T in (4) is investigated. The magnitude of the fitted multipliers are plotted in Fig. 3a with black dots together with the theoretical values (red vertical lines) as a function of the period r of the discretization. For a small discretization number, the DMD method can capture two complex conjugate pairs of multipliers having large magnitudes with good accuracy for these parameters in the example. On the other hand, taking into account more discretized points by increasing the discretization number, the fitted multipliers start to scatter leading to malicious modes. This scattering is related to the floating-point arithmetic and the accuracy of the numerical simulation (see the grey shaded area in Fig. 3a), which will be even more dominant in a real measurement process.

One way to select an appropriate number of discretization value, the singular values of the matrices $\mathbf{P}$ or $\mathbf{Q}$ can be analysed by determining a threshold below the singular values, which show a significant "drop" as proposed in [26,28,50,51]. In our paper, we use a different filtering approach detailed later.

The scattering multipliers are illustrated in the complex plane in Fig. 3b, also. As shown in the figure, the DMD method is not only able to capture the magnitude of the multipliers, but its imaginary and real components as well. However, a disadvantage of the proposed method is that it could not identify multipliers with small magnitude, since solution segments related to these terms are decaying rapidly. Hence, almost no information on these modes can be extracted and the convergence of these multipliers are limited by the floating-point arithmetic. Nevertheless, from the practical point of view, those are usually not relevant in engineering applications, since the stability is defined by the spectral radius (multiplier with the largest modulus: $|\mu_1|$).

In case of large discretization number, a possible way to eliminate the fitted malicious modes is to analyse the corresponding eigenvectors of the monodromy matrix Eq. (10). As shown in Fig. 4, in case of true modes, the mode shapes are smooth (see black curves), while for malicious modes, it contains large numerical noise (see grey curves), which is resulted by floating-point arithmetic. This numerical noise can be quantified by the standard deviation of the mode shape derivative (which is approximated by finite

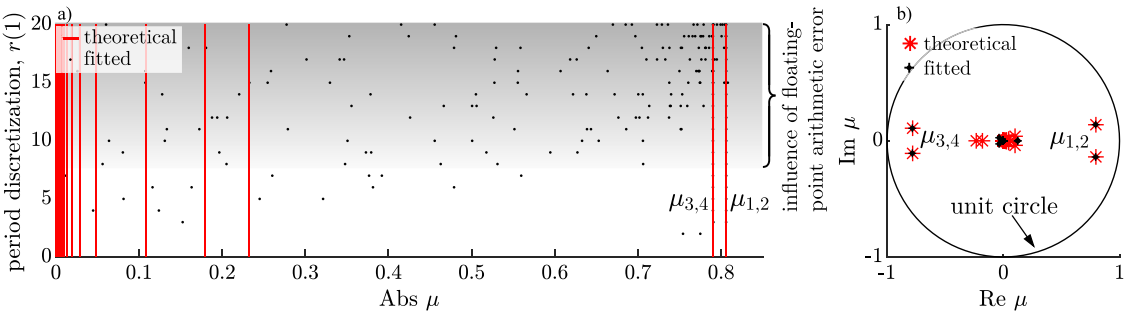

Fig. 3. Selection of an appropriate number of discretization value. Panel (a) shows the effect of discretization on fitted multipliers along the period while panel (b) represents dominant multipliers in the complex plane for parameters $n = 2$ and $K = 50$.

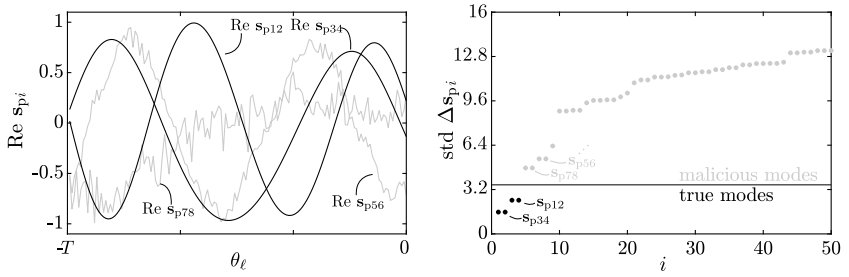

Fig. 4. Elimination of possible malicious modes. Panel (a) shows the computed eigenvectors of the first eight modes for parameters $r = 100$, $n = 2$ and $K = 50$. Panel (b) shows the standard deviation for the mode shape difference $\Delta s_j = (s_{j+1} - s_j)/\Delta t$.

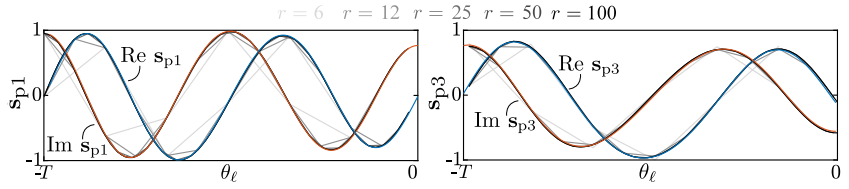

Fig. 5. The position component s_p of the two dominant eigenfunctions of operator $\mathcal{U}(T)$ in Eq. (3) (thick) and their different numerical counterparts $\mathbf{s}_p$ (thin greyscale). Note that all eigenvectors are normalized by the magnitude of their largest element $\|\mathbf{s}\|_\infty$. (For interpretation of the references to colour in this figure legend, the reader is referred to the web version of this article.)

difference). To determine this threshold value, one needs some intuition, although it has a small effect on the spectral radius, which is usually determined only by the modes with the smallest standard deviation. Thus, it is advisable to use a more strict limit for the filtering of the modes. It is important to note that the modes with the smallest standard deviation is not necessary the modes with the largest magnitude, which defines the spectral radius. As Fig. 4b shows that $|\mu_1| > |\mu_3|$, while $\mathrm{std}\,\Delta\mathbf{s}_1 < \mathrm{std}\,\Delta\mathbf{s}_3$.

Then, Fig. 5 shows that the discretized map in Eq. (5) approximates well the continuous time system Eq. (3) in terms of the dominant eigenvectors related to the largest two pairs of true multipliers (the malicious eigenvalues were eliminated based on the mode shapes as presented in Fig. 4). The coloured curves show the eigenfunctions $s_i(\theta)$ of operator $\mathcal{U}(T)$ in Eq. (3) approximated by the SDM method, while the greyscale curves are the mode shape vectors $\mathbf{s}$ of $\mathbf{U}$ in Eq. (10) for different discretization values r.

Finally, Fig. 6 presents the reconstructed signal according to the first and second dominant pairs of true multipliers $\mu_{1,2}$ and $\mu_{3,4}$ calculated by means of Eqs. (12) and (13). One can see that the amplitudes of the vibrations are in the same size as the original signal presented in Fig. 1, thus these two modes have large contributions.

Summarizing, by applying the DMD method to periodic systems, two numerical parameters are involved. One is the discretization of the signal along one period r, while the other one is how many periods are taken into account during the computation, denoted by K that should be larger than nr. Two computational problems may occur when using this method. One is how many periods are considered. On the one hand, to be able to use more points for the mode shape, more periods should be included. On the other hand, in case of a decaying signal, the numerical values in the umpteen periods are small, so their partiality is low, and thus, almost no information can be extracted from it. The other problem is how many points are considered in a period which leads to the appearance of malicious modes. From the engineering point of view, it is important to determine how reliable the fitted multipliers are. One way to decide it is to increase the number of discretization along one period, keeping in mind that large number of malicious modes will also appear which should be excluded later. The resolution of the eigenvectors depends also on the discretization number r.

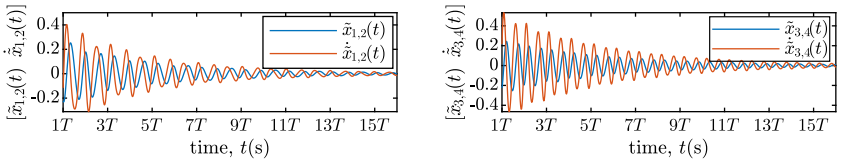

Fig. 6. Reconstructed time signals related to two dominant modes ($\mu_{1,2}$, $\mu_{3,4}$). (For interpretation of the references to colour in this figure legend, the reader is referred to the web version of this article.)

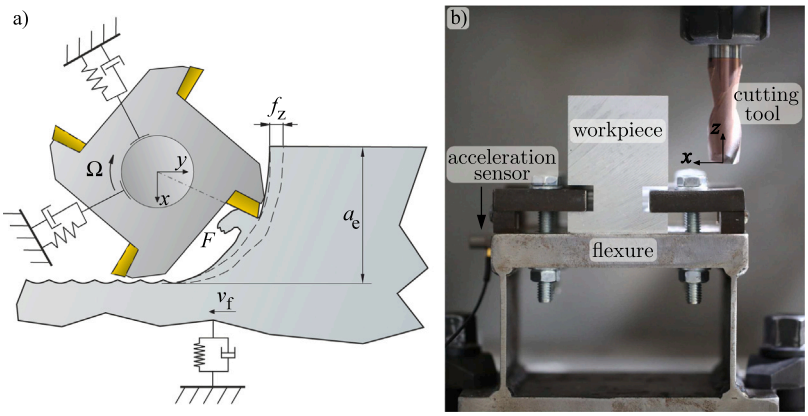

Fig. 7. Schematic of the mechanical model of the milling process (a) and the experimental setup (b).

The higher the discretization number is, the more points we can describe the eigenvector, thus, the 'smoother' the mode shapes we get. The multipliers and the mode shapes of these malicious modes will typically scatter for larger discretization, while they are converging for the true modes. Consequently, not only the multipliers but the mode shapes may involve additional information that can help to distinguish the true modes from the false ones.

4. Validation by experiment

In the followings, we give an insight into the efficiency of the proposed method by applying it to measured vibration data of a milling process. The intermittent nature of the cutting operation in milling clearly leads to delayed time-periodic system, in which the chatter detection and stability prediction are important engineering tasks.

4.1. Mechanical model of milling

In this subsection, the mechanical model of the milling process is discussed, on which the previously described model reduction technique is applied. Due to the complexity of the method, the mechanical model is kept as simple as possible while keeping the core elements of the dynamic behaviour.

The dynamical model with cylindrical milling tool is presented in Fig. 7a, which can be described in the modal space by using the vector of modal coordinates $\mathbf{q}(t) \in \mathbb{R}^d$ as

$$\ddot{\mathbf{q}}(t) + [2\zeta_k \omega_{\mathrm{n},k}]\dot{\mathbf{q}}(t) + [\omega_{\mathrm{n},k}^2]\mathbf{q}(t) = \mathbf{T}^{\top}\mathbf{F}(t, \mathbf{Tq}(t), \mathbf{Tq}(t-\tau)), \tag{16}$$

where $\mathbf{F}$ is the time-dependent cutting force, d is the number of degrees of freedom, and the modal parameters such as $\omega_{\mathrm{n},k}$, ζ_k and $\mathbf{T}$ are the kth natural angular frequency, the kth relative damping ratio and the mass normalized modal transformation matrix, respectively, and $[\cdot]$ refers to diagonal matrices.

The resultant cutting force has an explicit time dependency because it is proportional to the area of the chip cross-section which has time-periodic component due to the intermittent effects of the entering and exiting edges [3]. The dynamic chip thickness is influenced by the actual spatial position $\mathbf{x}(t) = \mathbf{Tq}(t)$ of the cutting edge position and the previous one $\mathbf{x}(t-\tau) = \mathbf{Tq}(t-\tau)$ due to the regenerative effect [4]. The time delay τ and the time period of the system in seconds $T(\mathrm{s}) = 2\pi/(\Omega(\mathrm{rad/s})Z)$ are equivalent ($\tau = T$) for the considered cutter with uniform pitch and inversely proportional to the spindle speed ($\Omega 60/(2\pi)$ in case of rpm). The reader is referred to [52] for a more detailed and general cutting force model of milling.

According to [23], the general solution $\mathbf{q}(t)$ of Eq. (16) can be written as a small perturbation $\mathbf{u}(t)$ around its periodic term $\mathbf{q}_{\mathrm{p}}(t)$ as

$$\mathbf{q}(t) = \mathbf{q}_{\mathrm{p}}(t) + \mathbf{u}(t), \tag{17}$$

where $\mathbf{q}_p(t) = \mathbf{q}_p(t+T)$ is T-periodic. The forced stationary periodic motion $\mathbf{q}_p(t)$ can be calculated from the particular solution of Eq. (16) as the solution of the following ordinary differential equation (ODE)

$$\ddot{\mathbf{q}}_p(t) + [2\zeta_k\omega_{n,k}]\dot{\mathbf{q}}_p(t) + [\omega_{n,k}^2]\mathbf{q}_p(t) = \mathbf{T}^\top\mathbf{G}(t), \tag{18}$$

where $\mathbf{G}(t) = \mathbf{G}(t+T) = \mathbf{F}(t, \mathbf{0}, \mathbf{0})$ is a T-periodic directional force coefficient [3].

The linear stability of this stationary periodic motion $\mathbf{q}_p(t)$ can be analysed through the variational delay differential equation of Eq. (16). It is derived by substituting Eq. (17) into Eq. (16), expanding it into Taylor series of the cutting force function and eliminating the higher-order terms, which leads to

$$\ddot{\mathbf{u}}(t) + [2\zeta_k\omega_{n,k}]\dot{\mathbf{u}}(t) + [\omega_{n,k}^2]\mathbf{u}(t) = \mathbf{T}^\top\Delta\mathbf{F}(t, \mathbf{T}\mathbf{u}(t), \mathbf{T}\mathbf{u}(t-\tau)), \tag{19}$$

where $\Delta\mathbf{F}(t, \mathbf{T}\mathbf{u}(t), \mathbf{T}\mathbf{u}(t-\tau))$ is the state dependent variational cutting force function. Therefore, Eq. (19) is a linear time-periodic delay differential equation (DDE). This form is compatible to Eq. (1), thus, according to the Floquet theory of DDEs [7], the stability is determined by the corresponding monodromy operator $\mathcal{U}(T)$.

4.2. Experimental setup

The applicability of the proposed method is investigated based on a widely-used setup [37,53–55], for which the corresponding mechanical model of the milling process is well-developed. The experimental setup is a single-degree-of-freedom (SDoF) flexible structure, which is considered from the work in [42] as the base of the measurement evaluation, shown in Fig. 7b. The machined workpiece is placed on a test-rig, which was designed to mimic the dynamics of a SDoF system. In this way, the signal-to-noise ratio can be kept in an acceptable range. The fitted modal parameters of the SDoF system are modal mass $m = 2.701$ kg, damping ratio $\zeta = 0.71\%$ and natural frequency $f_n = 259.96$ Hz ($\omega_n = 2\pi f_n = 1633.4$ rad/s). The selected machined material was aluminium 2024-T351, and the resultant radial and tangential force coefficients are $K_r = 1723$ MPa and $K_t = 2203$ MPa, respectively, as measured in [42]. During the milling experiments, the rest of the parameters were set as follows: feed per tooth $f_Z = 0.05$ mm/tooth and radial immersion $a_e = 2$ mm, TIVOLY P615H endmill with $Z = 2$ number of edges, diameter $D = 16$ mm, helix angle $\beta = 30°$ and rake angle $\kappa = 90°$ were used.

During the experiment, the cutting tests were carried out with a down-milling operation on a three-axis machine tool NCT EMR-610MS, where the cutting tool was mounted by BT30 ER25 spindle adapter. In the meantime, for sensing the vibrations, acceleration sensor PCB 352C23 was used and the data were acquired by NI cDAQ-9178 Chassis with NI 9234 Module at $f_s = 51\,200$ Hz sampling frequency. To visualize velocity and displacement signals, single and double integration in frequency domain were used together with an appropriate high-pass filter with cutoff frequency 50 Hz.

4.3. Triggering transient vibrations

Since the perturbation term is superposed onto the stationary solution (see Eq. (17)), it is necessary to perturb the system in some way. For operational stability prediction, one does not need to measure excitation since it only analyses the response. In-process impulse excitation for inducing transient vibration is used in [35,40] for mechanical structures, while in case of OMA, the excitation relies on the cutting force mainly and also on random ambient noise. For milling process, two excitation methods are proposed in [37] to trigger a transient vibration. One is based on the change in the cutting condition like tool's entry into the material or milling sharp corner [56]. The other one is an external impact perturbation where an additional hammer blow is applied during milling operation, which is further analysed in details in [42]. In this paper, we use hammer blow during the stationary cutting process, which has an advantage that it excites all the modes in the case of an ideal excitation. An alternative option for excitation can be a ball shooter device [57], which can be well automatized and has high repeatability capabilities [58].

To study the perturbation $\mathbf{u}(t)$, it is necessary to separate it from the stationary solution $\mathbf{q}_p(t)$ (see Eq. (17)). On the one hand, this can be done in the frequency domain by using the so-called comb filter, which is a widely used technique in the traditional chatter detection methods [19,59] and has also been used for stability prediction in [42]. However, separation of the forced vibration may have drawbacks meanwhile the associated frequency components are filtered by means of the comb filter. In some cases of flip or Hopf type stability losses, the frequency components related to the perturbation may be close to the forced vibration frequency. Therefore, during the filtering, frequency components relevant for stability may also be filtered.

On the other hand, the separation of the stationary solution can be done in the time domain as well by using an appropriate coordinate transformation. According to the so-called difference method proposed in [37,38], with the knowledge of the periodic component (before triggering the transient), it can be simply subtracted from the measured signal. However, this prior data collection limits the applicability. Automatic methods to subtract the periodic component without its prior direct measurement can be done based on, e.g., the moving integral method [40] or the application of homogeneous coordinate representation [60].

Fortunately, by using the DMD method proposed in this paper, it is not necessary to remove the periodic term from the measured signal beforehand. This term will automatically appear as a non-decaying standalone mode with corresponding multiplier $\mu_{per} = 1$ with a real periodic eigenvector $\mathbf{s}_{per}$, and in this way, it will be 'separated' from the total vibration signal. Consequently, the stability properties can be examined directly.

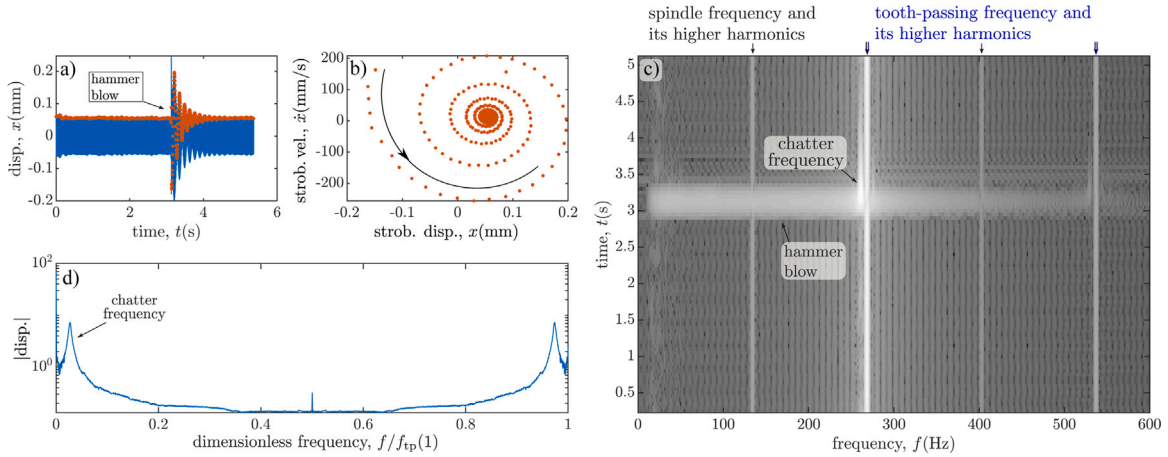

Fig. 8. Stable measurement behaviour near the stability boundary: time domain representation (panel a) and phase plane (panel b) of measured signal and its stroboscopic sections before and after hammer excitation. Panel (c) represents the wavelet transformation highlighting relevant frequency components and panel (d) shows the dimensionless spectrum of the stroboscopic sampling. Parameters are spindle speed 8052 rpm and axial depth of cut a_p = 1.5 mm. (For interpretation of the references to colour in this figure legend, the reader is referred to the web version of this article.)

4.4. Typical time signals near stability boundary

Several measurements were carried out for different technological parameters related to the material removal rate, such as the spindle speed and the axial depth of cut a_p. Out of dozens of experiments, we highlight and explain in details two different scenarios, which well characterize stable and unstable behaviour of the vibrations that occur near the stability limit. Time profiles, phase portraits together with their spectrograms (time–frequency diagrams) and dimensionless frequency spectra are visualized for stable and unstable milling operations near Hopf type stability losses in Figs. 8 and 9, respectively. In both figures, stroboscopic sampling according to Eq. (4) with $r = 1$ are visualized with red dots.

In Fig. 8a, one can see how the hammer blow excites the stationary solution at around 3 s. From this, the transient vibration develops, which dies out and the stationary solution returns again at around 5 s. This transient behaviour can also be seen in the stroboscopic sampled phase portrait in Fig. 8b, where the sampled points are spiralling back to the fixed point ($[x(T_i), \dot{x}(T_i)]$=[0.06 mm, 0 mm/s]) that belongs to the stable stationary solution. Fig. 8c represents the spectrogram of the signal, where the tooth-passing frequency $f_{tp} = 1/T$ and its higher harmonics are marked with blue arrows while the spindle frequency and its higher harmonics are shown with black arrows. These frequency components of the spectrum represent the stationary solution. It can be seen that a wide frequency range has been excited with the impulse excitation, from which most of the frequency components quickly disappear and only the one belonging to the chatter frequency survives, but it also decreases and completely vanishes at around 5 s as the transient vibration amplitude dies out. From this transient part, with the DMD method, one can identify the multipliers as a 'measure' of stability. Panel d) shows the fast fourier transformation of the stroboscopic sampled data, which characterizes well the range between the tooth-passing frequencies in the spectrogram.

Fig. 9 represents an unstable process close to the stability boundary. In this case, no excitation is needed since the noise from the cutting process causes enough perturbation to develop a transient vibration which appears as an outward spiral in panel b). Panel c) represents the spectrogram again, however, in contrast to the stable case in Fig. 8, there is an exponentially growing peak at the dominant chatter frequency. This exponential growth is limited mainly due to loss of contact (so-called fly-over effect) [61]. Namely, the vibration amplitude becomes so large that the cutting edges leave the material leading to saturated vibration amplitudes. This non-smooth behaviour can be traced by the appearance of additional peaks in the spectrum visible after 1.3 s.

For further examples near flip, fold and period-3 type stability loss scenarios, see Appendix.

4.5. Stability characterization

In contrast to the theory, one does not have prior information about the dominant vibration modes of the system. Furthermore, one cannot directly measure the general coordinates of Eq. (16), but only a few spatial coordinates due to the finite number of measurement points. Still, as in modal testing, a single measurement point can contain spectral information of all modes ($\omega_{n,k}, \zeta_k$) as long as the point is not a node. From measurement point of view, to extract characteristic multipliers, it is not even necessary to integrate and filter the measured acceleration signal, because it also contains dynamic information. Note that data acquisition method can greatly influence the results, such as data-sampling and signal-to-noise ratio. However, these challenges are not discussed in details as they are not directly related to the applicability of the proposed DMD method; they generally play an essential role in all measurement procedures. In what follows, the multipliers are extracted from a raw acceleration signal in case of an unstable milling process in Fig. 10a.

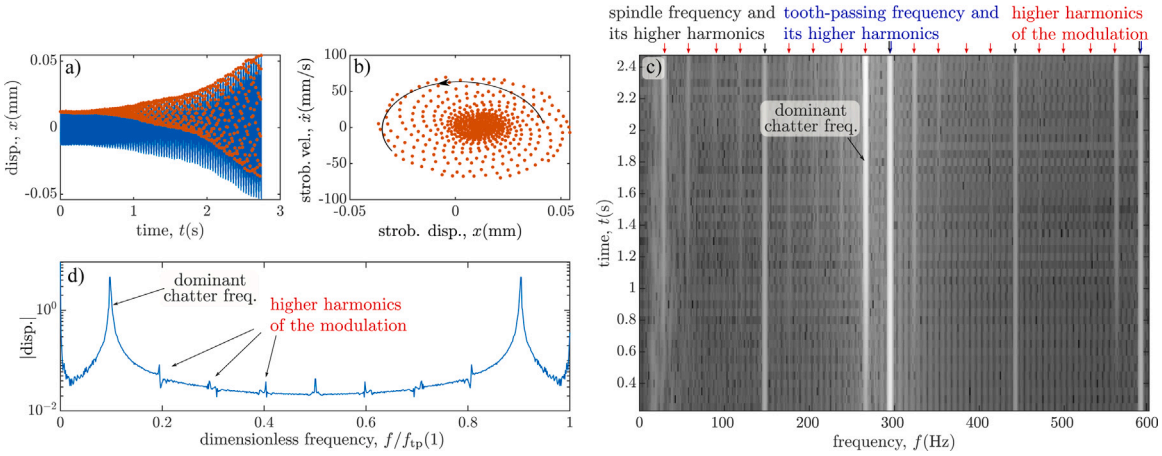

Fig. 9. Unstable measurement behaviour near the stability boundary: time domain representation (panel a) and phase plane (panel b) of measured signal and its stroboscopic sections before and after hammer excitation. Panel (c) represents the wavelet transformation highlighting relevant frequency components and panel (d) shows the dimensionless spectrum of the stroboscopic sampling. Parameters are spindle speed 8852 rpm and axial depth of cut $a_p = 1$ mm. (For interpretation of the references to colour in this figure legend, the reader is referred to the web version of this article.)

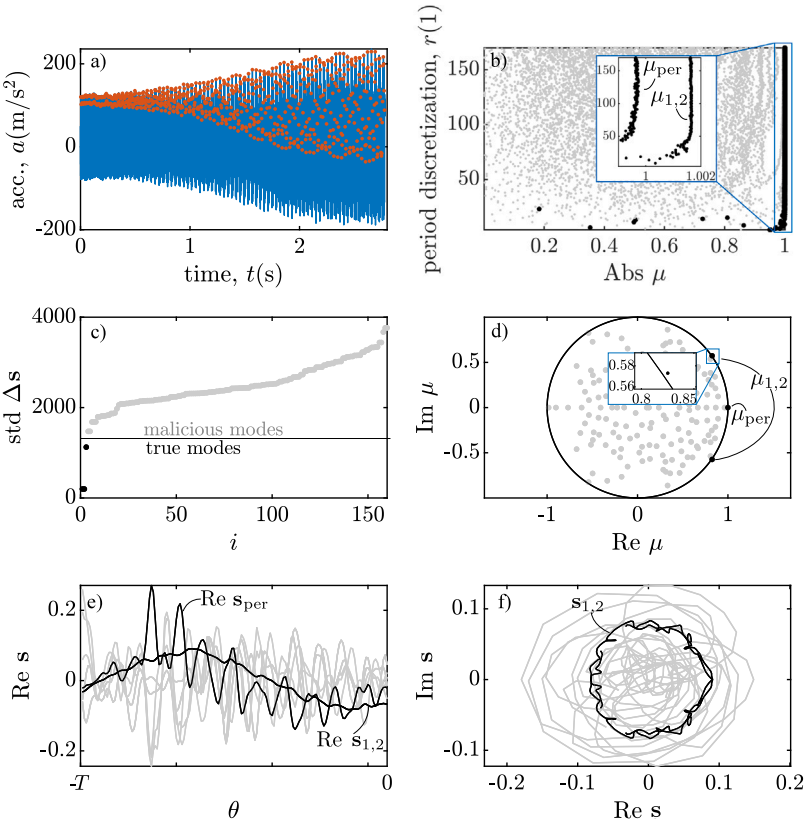

Fig. 10. Measured acceleration signal and the effects of the discretization in the DMD method. Panel (a) shows the time history of the used signal and its periodically sampled values. The true (black) and malicious (grey) multipliers are presented as the function of the period discretization in panel (b) and in the complex plane in panel (d). Panel (c) shows the deviation of the mode shapes while the fitted mode shapes are presented in panels (e) and (f). Parameters are spindle speed 8502 rpm, axial depth of cut $a_p = 1$ mm, $K = 180$, $n = 1$.

First, we examine the effect of sampling in Eq. (4) as well as the automatic selection of the malicious modes introduced in Section 3. The magnitude of the fitted true multipliers are plotted in panel (b) of Fig. 10 with black dots, while the excluded malicious multipliers are denoted by grey ones. Here, for each calculation, we select the first three multipliers as true ones because

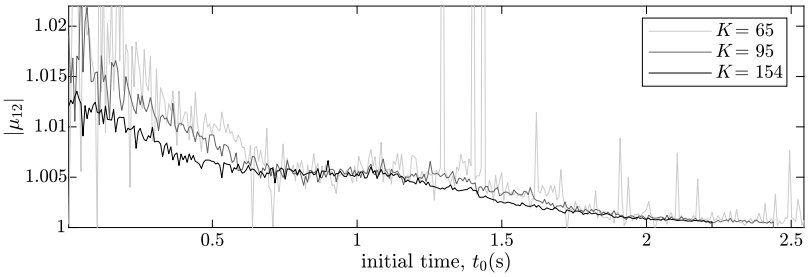

Fig. 11. Effects of the used time window for fitted true multipliers with parameters: spindle speed 8502 rpm, axial depth of cut $a_p = 1$ mm, $r = 50$. Note that parameters $K = 65$, 95 and 154 refer to time windows $T_w = 0.229$ s, 0.335 s and 0.543 s.

there was a change after it in the standard deviation of the corresponding mode shapes (see panel (c)). Note that the deviation of the third mode shape in Fig. 10c is close to the fourth and fifth modes. The reason for this is that the third mode is related to the periodic vibration term which contains larger frequency and this oscillation increases the value of the numerically calculated deviation. One can see in the enlarged panel that the true multipliers remain stable at a fixed location as r increases while the other ones begin to scatter around significantly, which can also be seen in the complex plane in panel (d). The DMD method provides a real characteristic multiplier with value one (μ_{per}) which refers to the stationary solution on which the unstable motion is superposed. The resulting dominant characteristic multipliers are a complex conjugate pair. Note this parameter combination is really close to the stability boundary leading to a slowly increasing amplitude and a small magnitude in characteristic multipliers $|\mu_{1,2}|$. The associated mode shapes ($\mathbf{s}_{per}$ and $\mathbf{s}_{1,2}$) are shown in panels of Fig. 10(e) and (f) illustrating their real parts and plotting these in the complex plane, respectively. Note that $\mathbf{s}_{per}$ has only real components, thus, in panel (e), it presents a time signal proportional to the periodic component. For further investigation, the discretization number along the period is fixed to $r = 50$, which gives a fairly accurate multiplier and can already describe the mode shapes appropriately. Note that during the identification of the dominant chatter frequency in milling processes, not only the multipliers but the mode shapes play a role [62].

The other free parameter in the DMD method is the number K of used periods. In case of real online chatter detection technique, this is referred to as the time window of the evaluated data. It means that the calculated multiplier will be delayed behind the actual measured data in case of online implementation. For fast chatter detection, a smaller time window (smaller K value) is preferred, while large value is expected to provide a more accurate and reliable 'measure' of stability. Consequently, it is an engineering task to balance between speed and accuracy/reliability. Furthermore, during online chatter detection, the selected time window is typically applied to the updated data, which is shifted forward in time.

In order to investigate the applicability of the method, the true multipliers are determined for different time windows while we shift the selected range along the transient part of the vibration. Fig. 11 presents the multiplier as a function of the initial time t_0 of the window for different window lengths T_w. It can be noticed that for too small time window, the reliability is poor, while larger time window can be thought of as a kind of averaging, which leads to smaller deviation. On the other hand, it should be noted that in the case of an unstable process, the exponential increase is limited after a while, and finally it tends to a large but finite amplitude vibration. If the time window covers these saturated parts, then the magnitude of the dominant multiplier might be underestimated. As one can see, the multiplier tends to 1 as the chatter vibration creates an attracting non-decaying large amplitude vibration. We can say, that the true dominant multiplier of the underlying linearized system is closer to the value detected at the beginning of the signal. This is, however, not so precise because the small initial unstable vibration is comparable to the measurement noise.

4.6. Wandering of multipliers

As it can be clearly seen in Fig. 10d, not only the spectral radius can be approximated, but also its imaginary parts. This provides a good opportunity to trace the wandering of the true multipliers in the complex plane as a function of technological parameters. Fig. 12 presents the fitted true multipliers $\mu_{1,2}$ together with the theoretically predicted counterparts in the complex plane for a set of different spindle speeds. It is presented for 3 different axial depth of cut $a_p = 1$, 1.5 and 2 mm. The theoretical multipliers are calculated by means of the SDM based on Eq. (19) for parameters presented in Section 4.2. The root locus curve as a function of spindle speed is denoted by continuous blue lines in Fig. 12.

For all panels, we start from a stable parameter domain and as the spindle speed is increased, the unstable domain is reached through a Hopf bifurcation. For stable spindle speeds (denoted by greenish stars), the measured values and the predicted ones are in good agreement. However, outside the unit circle in the unstable domain, the tendency of the fitted multipliers (reddish stars) does not follow the trend of the theory (blue line). A probable explanation for this is similar as described in the unstable case presented in Fig. 10, where the large amplitude vibration is saturated due to the fly-over effect. That is, there is no such exponential amplitude growth during the measurement that the theory would predict, leading to smaller magnitudes in the true multipliers. Note, that $\mu_{per} = 1$ is not shown in Fig. 12.

To check this amplitude saturation of the chatter vibration, we created an (experimental) bifurcation diagram by finding the peak-to-peak amplitude A_{per} of the stationary vibration and the peak-to-peak amplitude A_{chatt} of the chatter vibration after its saturation.

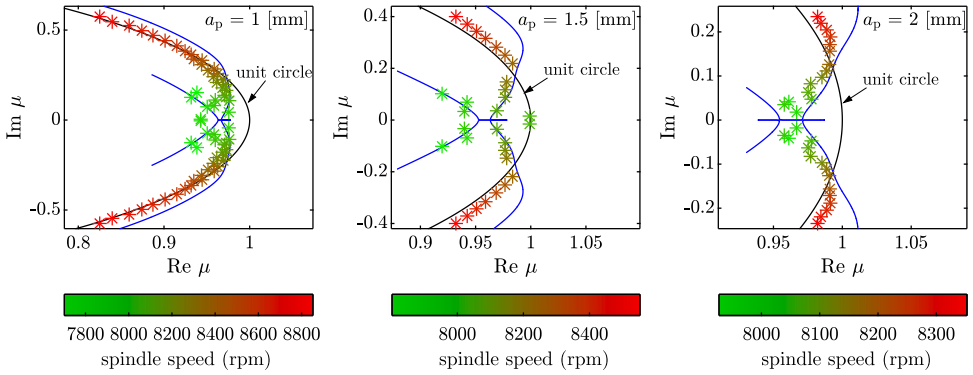

Fig. 12. Identified true multipliers for different spindle speeds (denoted by stars) in the complex plane compared to the path of the theoretical ones (continuous blue line) for axial depth of cut a_p = 1, 1.5 and 2 mm.. (For interpretation of the references to colour in this figure legend, the reader is referred to the web version of this article.)

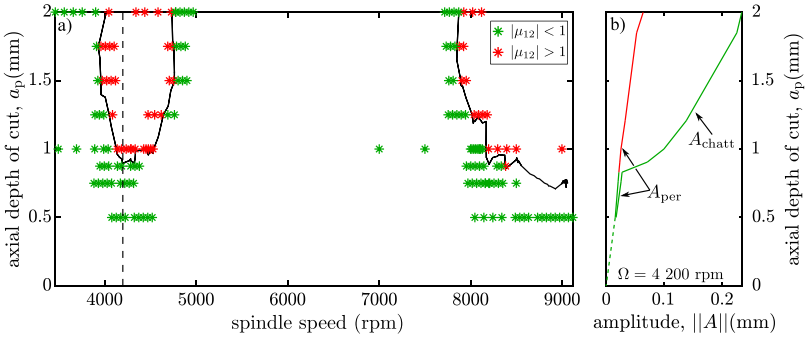

Fig. 13. (a) Complete stability chart prediction as the function of the technological parameters. Green and red stars denote stable ($|\mu_{1,2}| < 0$) and unstable ($|\mu_{1,2}| > 0$) milling operation while black contour-line shows the interpolated boundary. b) Measured bifurcation diagram determined by the reconstruction of the dominant component at around spindle speed is 4200 rpm. The green line represents attracting motions as stable cutting and chatter as a stable self-excited vibration, while the red line marks the unstable stationary solution. (For interpretation of the references to colour in this figure legend, the reader is referred to the web version of this article.)

The decomposition of the signal based on the corresponding modes was performed by the method described in Section 2.3. For a set of different axial depths of cut, we plot the amplitudes A_{per} and A_{chatt} and colour them according to their stability (see Fig. 13b). It can be seen that the stationary solution increases almost linearly with the depth of cut, as expected. However, as soon as unstable machining takes place at around a_p = 0.9 mm, a large amplitude solution appears related to a stable chaotic attractor. Based on the theory [61], this experimental bifurcation diagram should show subcritical Hopf bifurcation. However, for this, a more detailed measurement should be carried out around the bifurcation point. The corresponding bistable (unsafe) parameter regions were found in some previous measurements, which are analysed in details in [42]. Note that this type of bistable behaviour is also analysed in [63] by means of control-based continuation, where the Floquet multipliers and associated stable and unstable eigendirections were determined.

4.7. Interpolation and extrapolation of multipliers

As it is presented in the previous subsection, the change of the characteristic multiplier as a function of technological parameters can be followed with high accuracy. So it is possible to create an interpolation of the quantitative stability measure $|\mu_{1,2}|$ to reach much higher accuracy in the detection of the stability boundary. Furthermore, measuring the parameter plane of the stability chart, an accurate stability boundary can be generated by a contour-line at $|\mu_{1,2}| = 1$. The efficiency of this interpolation is shown in Fig. 13a, where a complete stability map is plotted along the technological parameters. This method opens the way for the measurement of the intricate shape of the stability chart through a course measurement grid only. Since the unstable multipliers can be underestimated due to the vibration amplitude saturation, the interpolation predicts a slightly larger stable domain. However, this is still a better quantitative forecast of the stability limit, than if one had a 'stable' or 'unstable' type qualitative estimation, from which the best possible interpolation is using the midpoint.

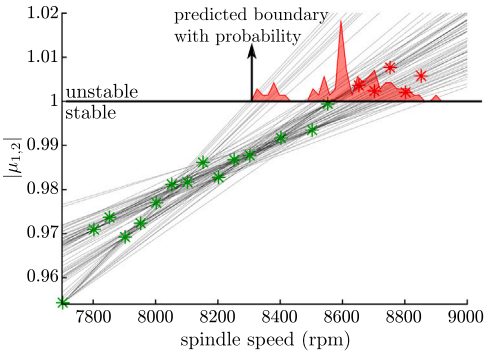

Fig. 14. Extrapolation method of the stability boundary based on stable measurement point-pairs. Green and red stars denote stable and unstable cutting condition, respectively, while black thin lines are fitted to two stable points used for extrapolation. Red shaded area characterizes the probability distribution of the different extrapolations. Parameter is axial depth of cut $a_p = 1$ mm. (For interpretation of the references to colour in this figure legend, the reader is referred to the web version of this article.)

On the stable side, the calculated multipliers show an excellent agreement with the theoretical values, since there is no underestimation due to nonlinear effects. It offers the possibility that the stability limit can be forecasted by extrapolation from stable accurate measurement points only. In Fig. 14, we present the magnitudes of the dominant stable/unstable multipliers $\mu_{1,2}$ with green/red stars as a function of the spindle speed presented in Fig. 12a. We fit lines to those points and created extrapolations based on the stable measurement points, only. The lines fitted onto two different points (see black thin lines) predict different spindle speeds for the stability limits when $|\mu_{1,2}| = 1$. We characterized the likelihood of the stability limit from these predicted points, which probability is visualized with the reddish shaded distribution function (histogram). The larger the value of the distribution function is, the greater the probability that the stability boundary is located at that spindle speed. The accuracy is better if we use points close to the stability boundary. But even the prediction based on measurement points at 7800 and 8200 rpm further away from the boundary can provide a fair approximation for the stability limit at around 8600 rpm. This extrapolation based on the DMD method can be used to determine the stability boundary without reaching harmful vibration on the machine tool. All these represent a rare situation when extrapolation can be more accurate than interpolation. However, it is fair to say in a possible online case the multipliers are time-dependent through the varying technological parameter leading to chatter. In this case dynamic bifurcation theory may also have importance [64].

5. Conclusions

In this contribution, it is shown by theoretical, numerical and experimental investigation that the Dynamic Modal Decomposition method is a proper tool for periodic dynamical systems to determine the stability behaviour from measured data. A stability measure from the approximated Floquet transition matrix is used to detect unstable cutting conditions in milling operation. This way, the Floquet theory meets the chatter detection technique.

Summarizing the steps of the method, first, one needs to split the signal by the principal period and then build the proper matrices for the DMD method. Then computing the pseudo inverse, the multipliers can be extracted, from which, malicious ones should be excluded by analysing the convergence of the modes and the deviation of the mode shapes.

During the test example and the measurement results, the exclusion of irrelevant and malicious multipliers based on standard deviation of the mode shape derivative seemed to be suitable. Although the method needs some parameters to be tuned, they are mostly related to the quality of the data acquisition system and not related to the threshold which separates stable and unstable operations like in case of traditional chatter detection methods. Some of the parameters of these traditional techniques need to be tuned even for noise-free signals. For measurement with proper quality, the tuning of our parameters has a slight influence on the identified spectral radius. Therefore, the proposed updated DMD method can effectively identify stable and unstable behaviour.

However, the essence of the proposed method is to estimate and forecast the stability limit while one can keep the technological parameters in stable machining condition, so ideally we can completely avoid unstable machining. The extrapolation of stability limit opens ways for efficient cutting parameter optimization strategies crossing the border towards reliable and optimal cutting.

It is still left for the future to examine the possibility of integrating the method in an online environment based on real-time signal processing that would be an essential element of active chatter suppression technique. Instead of a hammer blow, the applicability of alternative methods should also be studied, like the techniques based on operational modal analysis to improve manufacturing applicability.

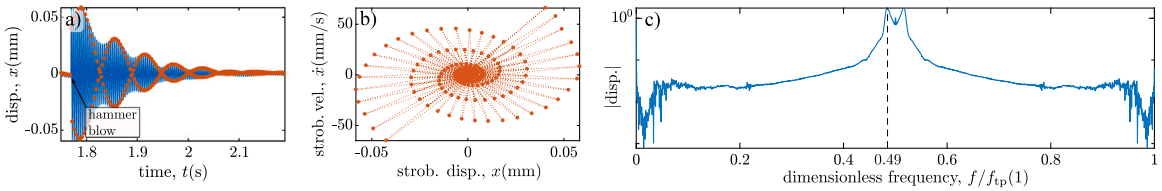

Fig. 15. Measured stable behaviour near flip bifurcation: panel (a) shows time domain representation of the measured signal before and after hammer excitation. Panel (b) presents the alternating behaviour of the stroboscopic sections in the phase portrait. Panel (c) shows the dimensionless spectrum of the stroboscopic sampling. Parameters are spindle speed 15 204 rpm and axial depth of cut $a_{\mathrm{p}} = 1.75$ mm.

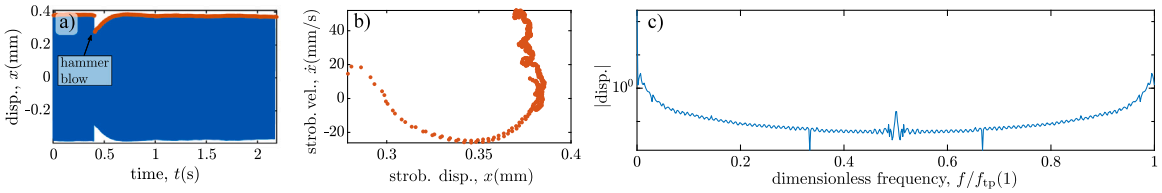

Fig. 16. Measured stable behaviour near fold bifurcation: panel (a) shows time domain representation of the measured signal before and after hammer excitation. Panel (b) presents the behaviour of the stroboscopic sections in the phase portrait. Panel (c) shows the dimensionless spectrum of the stroboscopic sampling. Parameters are spindle speed 8027 rpm and axial depth of cut $a_{\mathrm{p}} = 2$ mm.

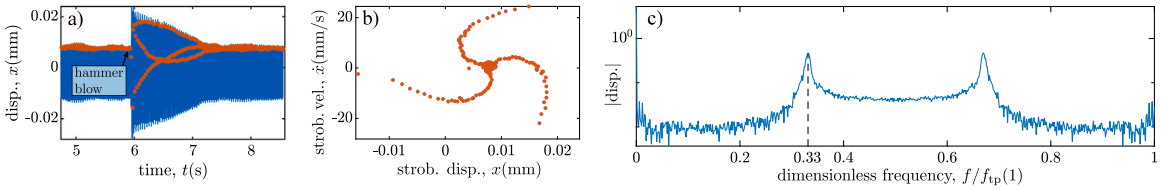

Fig. 17. Measured stable behaviour near period-3 type Hopf bifurcation: panel (a) shows time domain representation of the measured signal before and after hammer excitation. Panel (b) presents the behaviour of the stroboscopic sections in the phase portrait. Panel (c) shows the dimensionless spectrum of the stroboscopic sampling. Parameters are spindle speed 4826 rpm and axial depth of cut $a_{\mathrm{p}} = 1.25$ mm.

CRediT authorship contribution statement

Adam K. Kiss: Conceptualization, Methodology, Writing – original draft. **David Hajdu:** Validation. **Daniel Bachrathy:** Methodology, Supervision, Conceptualization. **Gabor Stepan:** Supervision, Funding acquisition. **Zoltan Dombovari:** Supervision, Funding acquisition.

Declaration of competing interest

The authors declare that they have no known competing financial interests or personal relationships that could have appeared to influence the work reported in this paper.

Acknowledgement

The research reported in this paper has been supported by the National Research, Development and Innovation Fund, Hungary (TKP2020 NC, Grant No. BME-NCS and TKP2021, Project no. BME-NVA-02) under the auspices of the Ministry for Innovation and Technology and by the Hungarian National Research, Development and Innovation Office (Grant no. NKFI FK-124462, NKFI PD-137673 and NEMZ:2019-2.1.2-NEMZ-2019-00005).

Appendix. Flip, fold, period-3

Figs. 15, 16 and 17 represent further typical stable time signals near flip, fold and period-3 type stability boundaries, respectively. Close to flip type (period-doubling) stability loss, the arising dominant chatter frequency is approximately half of the tooth-passing one. It means double time period of the tooth-passing one, which appears alternating stroboscopic sections in Fig. 15b. In case of fold type stability loss there is no additional chatter frequency in the spectrum, as it can be seen in Fig. 16c. It is known that based on the mathematical models only Hopf and flip-type stability losses can occur. However, the dominant multiplier with largest

modulus inside the stable domain can be a positive real multiplier, which results in a fast exponential decay. This can be observed in the experiments. While Fig. 17 presents a special case close to a Hopf bifurcation, where the frequency of the chatter vibration is one third of the tooth-passing one.

References

[1] J. Munoa, X. Beudaert, Z. Dombovari, Y. Altintas, E. Budak, C. Brecher, G. Stepan, Chatter suppression techniques in metal cutting, CIRP Ann-Manuf. Technol. 65 (2) (2016) 785–808, http://dx.doi.org/10.1016/j.cirp.2016.06.004.

[2] Y. Caixu, G. Haining, L. Xianli, S.Y. Liang, W. Lihui, A review of chatter vibration research in milling, Chin. J. Aeronaut. 32 (2) (2019) 215–242, http://dx.doi.org/10.1016/j.cja.2018.11.007.

[3] Y. Altintas, Manufacturing Automation - Metal Cutting Mechanics, Machine Tool Vibrations and CNC Design, Cambridge University Press, Cambridge, 2012, http://dx.doi.org/10.1017/CBO9780511843723,

[4] J. Tlusty, L. Spacek, Self-Excited Vibrations on Machine Tools, Nakl. CSAV, Prague. in Czech., 1954.

[5] S. Tobias, Machine-Tool Vibration, J. Wiley, Blackie, Glasgow, 1965, http://dx.doi.org/10.1049/tpe.1964.0084.

[6] G. Stepan, Retarded Dynamical Systems, Longman, Harlow, 1989.

[7] M. Farkas, Periodic Motions, Vol. 104, Springer-Verlag, New York, 1994, http://dx.doi.org/10.1007/978-1-4757-4211-4.

[8] T. Insperger, D. Lehotzky, G. Stepan, Regenerative delay, parametric forcing and machine tool chatter: A review, IFAC-PapersOnLine 48 (12) (2015) 322–327, http://dx.doi.org/10.1016/j.ifacol.2015.09.398.

[9] M.H. Kurdi, T.L. Schmitz, R.T. Haftka, B.P. Mann, A numerical study of uncertainty in stability and surface location error in high-speed milling, in: ASME International Mechanical Engineering Congress and Exposition, Vol. 42231, 2005, pp. 387–395, http://dx.doi.org/10.1115/IMECE2005-80875.

[10] X. Zhang, L. Zhu, D. Zhang, H. Ding, Y. Xiong, Numerical robust optimization of spindle speed for milling process with uncertainties, Int. J. Mach. Tools Manuf. 61 (2012) 9–19, http://dx.doi.org/10.1016/j.ijmachtools.2012.05.002.

[11] E. Graham, M. Mehrpouya, R. Nagamune, S. Park, Robust prediction of chatter stability in micro milling comparing edge theorem and LMI, CIRP J. Manuf. Sci. Technol. 7 (2014) 29–39, http://dx.doi.org/10.1016/j.cirpj.2013.09.002.

[12] D. Hajdu, F. Borgioli, W. Michiels, T. Insperger, G. Stepan, Robust stability of milling operations based on pseudospectral approach, Int. J. Mach. Tools Manuf. 149 (2020) 103516, http://dx.doi.org/10.1016/j.ijmachtools.2019.103516.

[13] Z. Dombovari, J. Munoa, R. Kuske, G. Stepan, Milling stability for slowly varying parameters, Proc. CIRP 77 (2018) 110–113, http://dx.doi.org/10.1016/j.procir.2018.08.233, 8th CIRP Conference on High Performance Cutting (HPC 2018).

[14] G. Quintana, J. Ciurana, Chatter in machining processes: A review, Int. J. Mach. Tools Manuf. 51 (2011) 363–376, http://dx.doi.org/10.1016/j.ijmachtools.2011.01.001.

[15] Y. Altintas, P.K. Chan, In-process detection and suppression of chatter in milling, Int. J. Mach. Tools Manuf. 32 (3) (1992) 329–347, http://dx.doi.org/10.1016/0890-6955(92)90006-3.

[16] E. Kuljanic, G. Totis, M. Sortino, Development of an intelligent multisensor chatterdetection system in milling, Mech. Syst. Signal Proc. 23 (2009) 1704–1718, http://dx.doi.org/10.1016/j.ymssp.2009.01.003.

[17] Y. Fu, Y. Zhang, H. Zhou, D. Li, H. Liu, H. Qiao, X. Wang, Timely online chatter detection in end milling process, Mech. Syst. Signal Proc. 75 (2016) 668–688, http://dx.doi.org/10.1016/j.ymssp.2016.01.003.

[18] A. Honeycutt, T.L. Schmitz, A new metric for automated stability identification in time domain milling simulation, J. Manuf. Sci. Eng. 138 (074501) (2016) http://dx.doi.org/10.1115/1.4032586.

[19] T. Delio, J. Tlusty, S. Smith, Use of audio signals for chatter detection and control, J. Eng. Ind. 114 (2) (1992) 146–157, http://dx.doi.org/10.1115/1.2899767.

[20] T.L. Schmitz, Chatter recognition by a statistical evaluation of the synchronously sampled audio signal, J. Sound Vib. 262 (2003) 721–730, http://dx.doi.org/10.1016/S0022-460X(03)00119-6.

[21] E. Kuljanic, M. Sortino, G. Totis, Multisensor approaches for chatter detection in milling, J. Sound Vib. 312 (2008) 672–693, http://dx.doi.org/10.1016/j.jsv.2007.11.006.

[22] Y. Ji, X. Wang, Z. Liu, H. Wang, L. Jiao, D. Wang, S. Leng, Early milling chatter identification by improved empirical mode decomposition and multi-indicator synthetic evaluation, J. Sound Vib. 433 (2018) 138–159, http://dx.doi.org/10.1016/j.jsv.2018.07.019.

[23] T. Insperger, G. Stepan, Semi-Discretization for Time-Delay Systems, in: Applied Mathematical Sciences, vol. 178, Springer, New York, 2011, http://dx.doi.org/10.1007/978-1-4614-0335-7.

[24] G. Scarciotti, A. Astolfi, Model reduction of neutral linear and nonlinear time-invariant time-delay systems with discrete and distributed delays, IEEE Trans. Automat. Control 61 (6) (2015) 1438–1451, http://dx.doi.org/10.1109/TAC.2015.2461093.

[25] W. Michiels, E. Jarlebring, K. Meerbergen, Krylov-based model order reduction of time-delay systems, SIAM J. Matrix Anal. Appl. 32 (4) (2011) 1399–1421, http://dx.doi.org/10.1137/100797436.

[26] A. Chatterjee, An introduction to the proper orthogonal decomposition, Curr. Sci. (2000) 808–817.

[27] Z. Dombovari, Dominant modal decomposition method, J. Sound Vib. 392 (2017) 56–69, http://dx.doi.org/10.1016/j.jsv.2016.12.012.

[28] Z. Dombovari, Stability properties of regenerative cutting processes, based on impulse response functions expressed in the impulse dynamic subspace, Int. J. Mach. Tools Manuf. 162 (2021) 103691, http://dx.doi.org/10.1016/j.ijmachtools.2021.103691.

[29] A.K. Kiss, D. Bachrathy, Z. Dombovari, Parameter identification of periodic systems by impulse dynamic subspace description, in: 10th European Nonlinear Dynamics Conference, ENOC 2020, Lyon, France, 2020.

[30] P.J. Schmid, Dynamic mode decomposition of numerical and experimental data, J. Fluid Mech. 656 (2010) 5–28, http://dx.doi.org/10.1017/S0022112010001217.

[31] B.W. Brunton, L.A. Johnson, J.G. Ojemann, J.N. Kutz, Extracting spatial–temporal coherent patterns in large-scale neural recordings using dynamic mode decomposition, J. Neurosci. Methods 258 (2016) 1–15, http://dx.doi.org/10.1016/j.jneumeth.2015.10.010.

[32] J.-C. Hua, S. Roy, J.L. McCauley, G.H. Gunaratne, Using dynamic mode decomposition to extract cyclic behavior in the stock market, Physica A 448 (2016) 172–180, http://dx.doi.org/10.1016/j.physa.2015.12.059.

[33] J.L. Proctor, P.A. Eckhoff, Discovering dynamic patterns from infectious disease data using dynamic mode decomposition, Int. Health 7 (2) (2015) 139–145, http://dx.doi.org/10.1093/inthealth/ihv009.

[34] J.L. Proctor, S.L. Brunton, J.N. Kutz, Dynamic mode decomposition with control, SIAM J. Appl. Dyn. Syst. 15 (1) (2016) 142–161, http://dx.doi.org/10.1137/15M1013857.

[35] K.D. Murphy, P.V. Bayly, L.N. Virgin, J.A. Gottwald, Measuring the stability of periodic attractors using perturbation-induced transients: Applications to two non-linear oscillators, J. Sound Vib. 172 (1994) 85–102, http://dx.doi.org/10.1006/jsvi.1994.1160.

[36] P. Bayly, L. Virgin, An empirical study of the stability of periodic motion in the forced spring-pendulum, Proc. R. Soc. Lond. Ser. A-Math. Phys. Eng. Sci. 443 (1918) (1993) 391–408, http://dx.doi.org/10.1098/rspa.1993.0152.

[37] B.P. Mann, K.A. Young, An empirical approach for delayed oscillator stability and parametric identification, Proc. R. Soc. Lond. Ser. A-Math. Phys. Eng. Sci. 462 (2006) 2145–2160, http://dx.doi.org/10.1098/rspa.2006.1677.
[38] S. Torkamani, E.A. Butcher, F.A. Khasawneh, Parameter identification in periodic delay differential equations with distributed delay, Commun. Nonlinear Sci. Numer. Simul. (ISSN: 1007-5704) 18 (4) (2013) 1016–1026, http://dx.doi.org/10.1016/j.cnsns.2012.09.001.
[39] B. Heizer, T. Kalmár-Nagy, Proper orthogonal decomposition and dynamic mode decomposition of delay-differential equations, IFAC-PapersOnLine 51 (14) (2018) 254–258, http://dx.doi.org/10.1016/j.ifacol.2018.07.232.
[40] J.A. Little, J.D. Turner, B.P. Mann, Improving empirical characteristic multiplier estimation through a change of basis, J. Sound Vib. (ISSN: 0022-460X) 488 (2020) 115613, http://dx.doi.org/10.1016/j.jsv.2020.115613.
[41] J.H. Tu, C.W. Rowley, D.M. Luchtenburg, S.L. Brunton, J.N. Kutz, On dynamic mode decomposition: Theory and applications, J. Comput. Dyn. 1 (2) (2014) 391–421, http://dx.doi.org/10.3934/jcd.2014.1.391.
[42] A.K. Kiss, D. Bachrathy, G. Stepan, Operational stability prediction in milling based on impact tests, Mech. Syst. Signal Proc. 103 (2018) 327–339, http://dx.doi.org/10.1016/j.ymssp.2017.10.019.
[43] S. Kim, K. Ahmadi, Estimation of vibration stability in turning using operational modal analysis, Mech. Syst. Signal Proc. 130 (2019) 315–332, http://dx.doi.org/10.1016/j.ymssp.2019.04.057.
[44] E.A. Butcher, O.A. Bobrenkov, E. Bueler, P. Nindujarla, Analysis of milling stability by the Chebyshev collocation method: algorithm and optimal stable immersion levels, J. Comput. Nonlinear Dyn. 4 (031003) (2009) http://dx.doi.org/10.1115/1.3124088.
[45] F.A. Khasawneh, B.P. Mann, A spectral element approach for the stability of delay systems, Internat. J. Numer. Methods Engrg. 87 (2011) 566–952, http://dx.doi.org/10.1002/nme.3122.
[46] P.V. Bayly, J.E. Halley, B.P. Mann, M.A. Davies, Stability of interrupted cutting by temporal finite element analysis, J. Manuf. Sci. Eng. 125 (2003) 220–225, http://dx.doi.org/10.1115/DETC2001/VIB-21581.
[47] D. Breda, S. Maset, R. Vermiglio, Stability of Linear Delay Differential Equations: A Numerical Approach with MATLAB, Springer, 2015, http://dx.doi.org/10.1007/978-1-4939-2107-2.
[48] T. Insperger, G. Stepan, Stability chart for the delayed Mathieu equation, Proc. R. Soc. London Ser. A-Math. Phys. Eng. Sci. 458 (2024) (2002) 1989–1998, http://dx.doi.org/10.1098/rspa.2001.0941.
[49] T. Insperger, G. Stepan, Stability of the damped mathieu equation with time delay, J. Dyn. Syst. Meas. Control-Trans. ASME 125 (2003) 166–171, http://dx.doi.org/10.1115/1.1567314.
[50] G. Quaranta, P. Mantegazza, P. Masarati, Assessing the local stability of periodic motions for large multibody non-linear systems using proper orthogonal decomposition, J. Sound Vib. 271 (3–5) (2004) 1015–1038, http://dx.doi.org/10.1016/j.jsv.2003.03.004.
[51] X. Zhao, B. Ye, Selection of effective singular values using difference spectrum and its application to fault diagnosis of headstock, Mech. Syst. Signal Proc. 25 (5) (2011) 1617–1631, http://dx.doi.org/10.1016/j.ymssp.2011.01.003.
[52] M. Zatarain, Z. Dombovari, Stability analysis of milling with irregular pitch tools by the implicit subspace iteration method, Int. J. Dyn. Control 2 (2014) 26–34, http://dx.doi.org/10.1007/s40435-013-0052-7.
[53] P.V. Bayly, B.P. Mann, T.L. Schmitz, D.A. Peters, G. Stepan, T. Insperger, Effects of radial immersion and cutting direction on chatter instability in end-milling, in: ASME International Mechanical Engineering Congress and Exposition, Vol. 3641, 2002, pp. 351–363, http://dx.doi.org/10.1115/IMECE2002-39116.
[54] T. Ransom, A. Honeycutt, T. Schmitz, A new tunable dynamics platform for milling experiments, Precis. Eng. 44 (2016) 252–256, http://dx.doi.org/10.1016/j.precisioneng.2016.01.005.
[55] J. Munoa, M. Sanz-Calle, Z. Dombovari, A. Iglesias, J. Pena-Barrio, G. Stepan, Tuneable clamping table for chatter avoidance in thin-walled part milling, CIRP Ann-Manuf. Technol. 69 (1) (2020) 313–316, http://dx.doi.org/10.1016/j.cirp.2020.04.081.
[56] A.K. Kiss, D. Bachrathy, Dynamic characterization of milling based on interrupted feed motion, MM Sci. J. (2021) 5142–5147, http://dx.doi.org/10.17973/MMSJ.2021_11_2021170.
[57] D. Takács, R. Wohlfart, A. Miklós, G. Krajnyák, A. Tóth, G. Stépán, Ball shooting tests for identification of modal parameter variation in rotating main spindles, Proc. CIRP 77 (2018) 481–484, http://dx.doi.org/10.1016/j.procir.2018.08.260.
[58] D. Bachrathy, A.K. Kiss, A. Kossa, S. Berezvai, D. Hajdu, G. Stepan, In-process monitoring of changing dynamics of a thin-walled component during milling operation by ball shooter excitation, J. Manuf. Mater. Process. 4 (3) (2020) 78, http://dx.doi.org/10.3390/jmmp4030078.
[59] D. Aslan, Y. Altintas, On-line chatter detection in milling using drive motor current commands extracted from CNC, Int. J. Mach. Tools Manuf. 132 (2018) 64–80, http://dx.doi.org/10.1016/j.ijmachtools.2018.04.007.
[60] A.K. Kiss, D. Bachrathy, G. Stepan, Experimental determination of dominant multipliers in milling process by means of homogeneous coordinate transformation, in: International Design Engineering Technical Conferences and Computers and Information in Engineering Conference, Vol. 58226, American Society of Mechanical Engineers, 2017, http://dx.doi.org/10.1115/DETC2017-67827, V008T12A053.
[61] Z. Dombovari, A. Iglesias, T.G. Molnar, G. Habib, J. Munoa, R. Kuske, G. Stepan, Experimental observations on unsafe zones in milling processes, Philos. Trans. R. Soc. A-Math. Phys. Eng. Sci. 377 (2153) (2019) 20180125, http://dx.doi.org/10.1098/rsta.2018.0125.
[62] Z. Dombovari, A. Iglesias, M. Zatarain, T. Insperger, Prediction of multiple dominant chatter frequencies in milling processes, Int. J. Mach. Tools Manuf. 51 (2011) 457–464, http://dx.doi.org/10.1016/j.ijmachtools.2011.02.002.
[63] D.A.W. Barton, Control-based continuation: Bifurcation and stability analysis for physical experiments, Mech. Syst. Signal Proc. 84 (2017) 54–64, http://dx.doi.org/10.1016/j.ymssp.2015.12.039.
[64] S.M. Baer, T. Erneux, J. Rinzel, The slow passage through a Hopf bifurcation: delay, memory effects, and resonance, SIAM J. Appl. Math. 49 (1) (1989) 55–71, http://dx.doi.org/10.1137/0149003.